Journal of Magnetism and Magnetic Materials 149 (1995) 143–147

ELSEVIER

Journal of magnetism and magnetic materials

Dynamics of a magnetic fluid droplet in a rotating field

J.C. Bacri [a,*], A. Cebers [b], S. Lacis [b], R. Perzynski [a]

[a] *Lab. AOMC (Assoc. CNRS), Université P.M. Curie, 4 place Jussieu, 75252 Paris Cedex 05, France*
[b] *Latvian Academy of Sciences, Institute of Physics, Salaspils-1, LV-2169, Latvia*

Abstract

The response of a magnetic fluid microdrop to a rotating magnetic field is studied numerically in 2D by the boundary element method (BEM). On increasing field frequency, the motion of the droplet goes through a transition from a state where the droplet follows the magnetic field with a constant phase lag to a state where the phase lag increases in a series of kinks when the field frequency passes the critical one. The equations of the droplet motion are derived analytically and good agreement with the BEM is obtained.

It is well known that for a rigid magnetic dipole there is a critical angular velocity of the rotating field below which the rotation of particle and field are synchronized [1]. Similar phenomena are observed for a bound pair of soft magnetic particles [2,3]. The interplay between magnetic and viscous forces leads to various modes of motion, which in Refs. [2,3] are classified as (1) steady-state rotations; (2) 'jerky' (rotations with stops and backward motions); and (3) localized oscillations. Transitions between these modes are well described by a single non-linear equation and depend on the frequency and amplitude of the rotating field, the fluid viscosity and the magnetic susceptibility. It is found both experimentally and numerically [3] that for a pair of free spheres phase locking takes place in an elliptical polarized field $\bar{\Omega}/\Omega_H = 1/2, 1/4$, etc., where $\bar{\Omega}$ is the average angular frequency of the pair-rotation and Ω_H is the angular frequency of the magnetic field rotation. The magnetic fluid (MF) microdroplet in the rotating magnetic field includes a wide variety of very complex phenomena in the high-frequency range [4]. In the low-frequency range, an elongated droplet rotates with magnetic field frequency, with the surface tension playing an equivalent role to that of the soft binding in a pair of magnetic spheres.

The scope of the present paper is the behaviour of the MF droplet in the intermediate frequency range of a rotating magnetic field, studied by a numerical simulation. In the two-dimensional (2D) case, we apply the boundary integral equation technique (BEM: the boundary element method) considered previously in Refs. [5,6]. We assume that the magnetic permeability is constant (μ = const), and that gravity and inertia forces are negligible due to the very small size of the droplet. Hence the effective surface forces have only the following normal component:

$$f_s^n = \sigma/R_L - (\mu - 1)(\mu H_n^2 + H_t^2)/(8\pi). \tag{1}$$

Here σ is the surface tension, R_L is the local curvature radius, and μ is the magnetic permeability of the MF. Both the normal and tangential components H_n, H_t of the magnetic field strength on the boundary are found as solutions of the corresponding boundary integral equations [5]:

$$H_n|_\Gamma = \frac{2H_{0X}}{(\mu+1)}\frac{\partial x}{\partial n} + \frac{2H_{0Y}}{(\mu+1)}\frac{\partial y}{\partial n} + \frac{1}{\pi}\frac{(\mu-1)}{(\mu+1)} \times \oint_L H_n(l')|_\Gamma K(\boldsymbol{r}, \boldsymbol{r}')\frac{dl'}{\sqrt{x_l^2 + y_l^2}}, \tag{2}$$

$$H_t|_\Gamma = \frac{2H_{0X}}{(\mu+1)}\frac{\partial x}{\partial l} + \frac{2H_{0Y}}{(\mu+1)}\frac{\partial y}{\partial l} - \frac{1}{\pi}\frac{(\mu-1)}{(\mu+1)} \times \oint_L H_t(l')|_\Gamma K(\boldsymbol{r}, \boldsymbol{r}')\frac{dl'}{\sqrt{x_l^2 + y_l^2}}, \tag{3}$$

$$K(\boldsymbol{r}, \boldsymbol{r}') = \frac{x_l(y'-y) - y_l(x'-x)}{(y'-y)^2 + (x'-x)^2}.$$

Calculated field components are used for effective surface forces (1). The surface motion is calculated using the potential theory of viscous flow, described in Refs. [7,8].

* Corresponding author. Email: jcbac@ccr.jussieu.fr; fax: +33-1-44273854. Affiliation: Université Paris VII.

The corresponding boundary integral equation for the velocity v of the fluid on the boundary of the droplet in 2D is

$$v_i(x) = -\frac{1}{2\pi(\eta_{ex}+\eta_{in})}\oint_L n_j f_s^n G_{ij}(x, x')\,dl' + \frac{\eta_{ex}-\eta_{in}}{4\pi(\eta_{ex}+\eta_{in})} \times \oint_L v_j(x') n_k(x') f_s^n T_{ijk}(x, x')\,dl', \quad (4)$$

where

$$G_{ij}(x, x') = -\delta_{ij}\ln|\hat{x}| + \frac{\hat{x}_i\hat{x}_j}{|\hat{x}|^2},$$

$$T_{ijk}(x, x') = -4\frac{\hat{x}_i\hat{x}_j\hat{x}_k}{|\hat{x}|^4}, \qquad \hat{x} = x' - x,$$

η stands for viscosity, the subscripts 'in' denotes the MF droplet and 'ex' the surrounding fluid. In the present paper only the results obtained by BEM for the case of equal viscosities ($\eta_{in} = \eta_{ex}$), are presented. In this case Eq. (4) simplifies to

$$v_i(x) = -\frac{1}{2\pi(\eta_{ex}+\eta_{in})}\oint_L n_j f_s^n G_{ij}(x, x')\,dl'. \quad (5)$$

The boundary contour is approximated by a finite number of marker points connected together by interpolating cubic spline functions. As in Ref. [6], the distance of marker points separation is proportional to the local radius of curvature within limits which prevent the absence of points at places on the contour with small curvature. This non-equidistant distribution of marker points gives a better accuracy at droplet tips where the contour curvature is larger.

The approximation technique for Eqs. (2), (3), (5), described in detail in Refs. [5,9], is based on linear interpolation of the corresponding unknowns (H_n, H_t, v_i) between marker points along the droplet contour and application of the Galerkin method. The singularities are subtracted and integrated analytically. The first and second derivatives along the boundary contour (x_l, x_{ll}, y_l, y_{ll}) are calculated by differentiating the corresponding cubic spline functions. For a rotating field we have $H_{0X} = H_0 \cos \Omega_H t$, $H_{0Y} = H_0 \sin \Omega_H t$. The sets of linear algebraic equations, obtained for Eqs. (2), (3) are solved using Gaussian elimination The approximation of (5) leads to a sum. In each time step, magnetic field components are calculated and applied for the surface movement velocity calculation. Once the velocity has been calculated, the position of the interface is advanced using an explicit Euler method. After each time step the droplet dimensions are rescaled to improve the volume conservation.

Further in this paper, a dimensionless form for physical parameters and geometric dimensions of droplet is used. The external field strength H_0, the surface tension σ, the external fluid viscosity η_{ex} and the unperturbed droplet (i.e. circle) radius R are chosen as characteristic values. Physical processes are characterized by the magnetic Bond number $B_m = H_0^2 R/\sigma$, the surface energy of a circular 2D droplet per unit length of a cylinder $E_c = 2\pi R\sigma$, the characteristic time interval for droplet motion $\tau = \eta_{ex} R/\sigma$

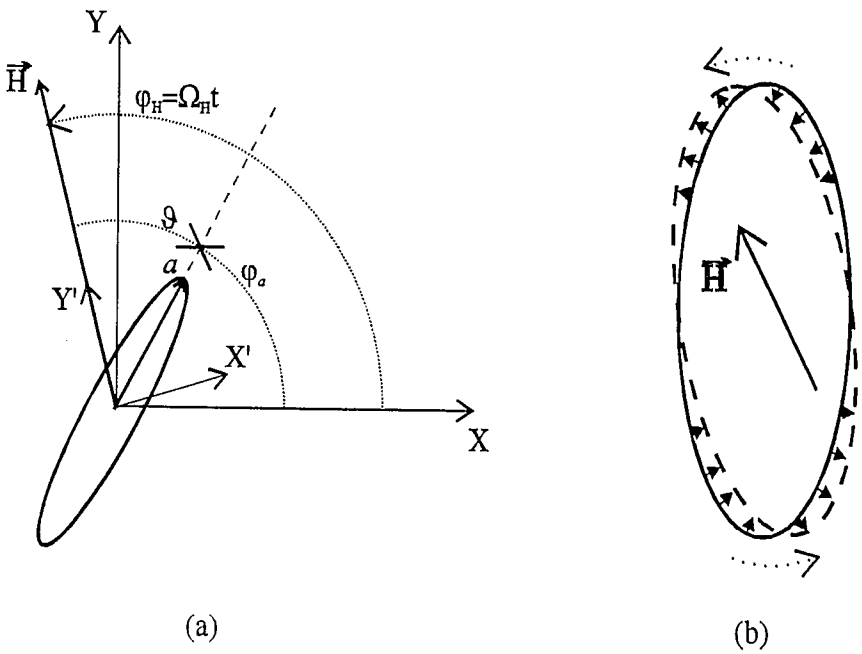

Fig. 1. (a) The orientation of a droplet with respect to the magnetic field and laboratory coordinates. (b) The wave-like perturbation propagation.

and the ratio of viscosities $\lambda = \eta_{in}/\eta_{ex}$. So we have dimensionless coordinates $\tilde{x} = x/R$, $\tilde{y} = y/R$, a dimensionless velocity $\tilde{v} = v\tau/R$, a dimensionless magnetic field $\boldsymbol{H} = \boldsymbol{H}/H_0$, a dimensionless frequency of field rotation $\tilde{\Omega} = \Omega\tau$ and a dimensionless time $\tilde{t} = t/\tau$. All the further formulae are written in a dimensionless form dropping the tilde; in special cases the dimensional form is denoted by a circumflex (^).

The behaviour of the MF droplet in a rotating magnetic field can be understood on the basis of a simple model, derived under the assumption of an elliptical shape of the 2D droplet. The configuration of the elliptical droplet is described by its large semi-axis $a = \hat{a}/R$ and the phase lag ϑ of the large semi-axis with respect to the field direction (see Fig. 1(a)). Let us separate the motion of the elliptical 2D droplet into two processes. The first is an extension–contraction motion caused by the surface tension and the magnetic field, acting on the droplet in a direction determinated by the phase lag ϑ. The total energy (magnetic plus surface contributions) of the elliptic 2D droplet [9] is, with respect to the field direction (in a dimensionless form),

$$E_1 = \frac{2a\mathrm{E}(e)}{\pi} - \frac{\mu-1}{16\pi}B_m\left(\frac{a^2+1}{a^2+\mu}\cos^2\vartheta + \frac{a^2+1}{a^2\mu+1}\sin^2\vartheta\right), \tag{6}$$

where

$$\mathrm{E}(e) = \int_0^{2\pi}\sqrt{1-(e\sin x)^2}\,\mathrm{d}x$$

is the complete elliptic integral of the first kind, $e^2 = 1 - b^2/a^2$.

In this process, the total energy changes are balanced by an energy dissipation in the viscous flow inside and outside the droplet:

$$\dot{E} = \dot{E}_{in} + \dot{E}_{ex} = \frac{\mathrm{d}E_t}{\mathrm{d}t} = \dot{a}\frac{\mathrm{d}E_t}{\mathrm{d}a}. \tag{7}$$

The energy dissipation inside the droplet is approximated as an homogeneous extension–contraction motion ($v_{x'} = x'\dot{a}/a$, $v_{y'} = -y'\dot{a}/a$, see Fig. 1(a) for x', y'). It gives

$$\dot{E}_{in} = -2\lambda(\dot{a}/a)^2. \tag{8}$$

For the energy dissipation outside the droplet the following approximation is used:

$$\dot{E}_{ex} = -2p(\dot{a}/a)^2, \tag{9}$$

where p is some phenomenological parameter of the model.

Collecting Eqs. (6)–(9) together, we obtain the droplet motion equation for large semi-axis a:

$$\dot{a} = \frac{a^2}{\pi(\lambda+p)}\left[\frac{(\mu-1)^2}{16}B_m a\left(\frac{\cos^2\vartheta}{(a^2+\mu)^2} - \frac{\sin^2\vartheta}{(\mu a^2+1)^2}\right) - \frac{\Phi(a)}{a^4-1}\right], \tag{10}$$

$$\Phi(a) = \left((a^4+1)\mathrm{E}(e) - 2\mathrm{K}(e)\right),$$

where

$$\mathrm{K}(e) = \int_0^{2\pi} 1/\sqrt{1-(e\sin x)^2}\,\mathrm{d}x$$

is the complete elliptic integral of the second kind.

The second process is the droplet rotation, characterized by the balance of the viscous and magnetic torques ($\hat{N}_f + \hat{N}_m = 0$). The viscous forces are determinated by a creeping flow around the rotating elliptic cylinder, which could be derived using the method described for a general ellipsoid in Ref. [10], modifying this method for the case of 2D. The obtained viscous torque (the dimensional z-component, per unit length of a cylinder) is

$$\hat{N}_f = -2\pi\hat{\eta}_{ex}\hat{\Omega}(\hat{a}^2+\hat{b}^2). \tag{11}$$

It has to be balanced by a magnetic torque

$$\hat{N}_m = \int_S \hat{\boldsymbol{M}}\,\mathrm{d}\hat{S}\times\hat{\boldsymbol{H}} = H_0^2\frac{\sin 2\vartheta}{8}\hat{a}\hat{b}\frac{(\mu-1)^2(\hat{a}^2-\hat{b}^2)}{(\hat{a}+\mu\hat{b})(\hat{a}\mu+\hat{b})}. \tag{12}$$

The angular frequency of an ellipse rotation in laboratory coordinates is (see Fig. 1(a) for the definitions of φ_a, φ_H)

$$\Omega = \dot{\varphi}_a = \dot{\varphi}_H - \dot{\vartheta} = \Omega_H - \dot{\vartheta}. \tag{13}$$

Collecting together Eqs. (11)–(13) we obtain the dimensionless droplet motion equation for the phase lag ϑ:

$$\dot{\vartheta} = \Omega_H - \Omega_{cr}\sin 2\vartheta, \tag{14}$$

where

$$\Omega_{cr} = \frac{B_m}{16\pi}\frac{(\mu-1)^2a^2(a^4-1)}{(a^2+\mu)(a^2\mu+1)(a^4+1)}.$$

At low magnetic field rotation frequencies Ω_H, the MF droplet rotates uniformly with a frequency equal to that of the field. Steady-state rotations are studied using both the BEM and the simple model, and the results for $\lambda = 1$ are shown in Fig. 2 in coordinates (x', y') which rotate together with the magnetic field so that the y'-axis is pointed in the field direction (see Fig. 1(a)). A typical number of marker points for BEM calculations is $N = 200$. For the simple model simulations, the value $p = 1$ is used. The solid curve in Fig. 2 represents the positions of the elliptic droplet tips for a continuously varying frequency Ω_H. The end of the large semi-axis with coordinates $x'_a = a\sin\vartheta$,

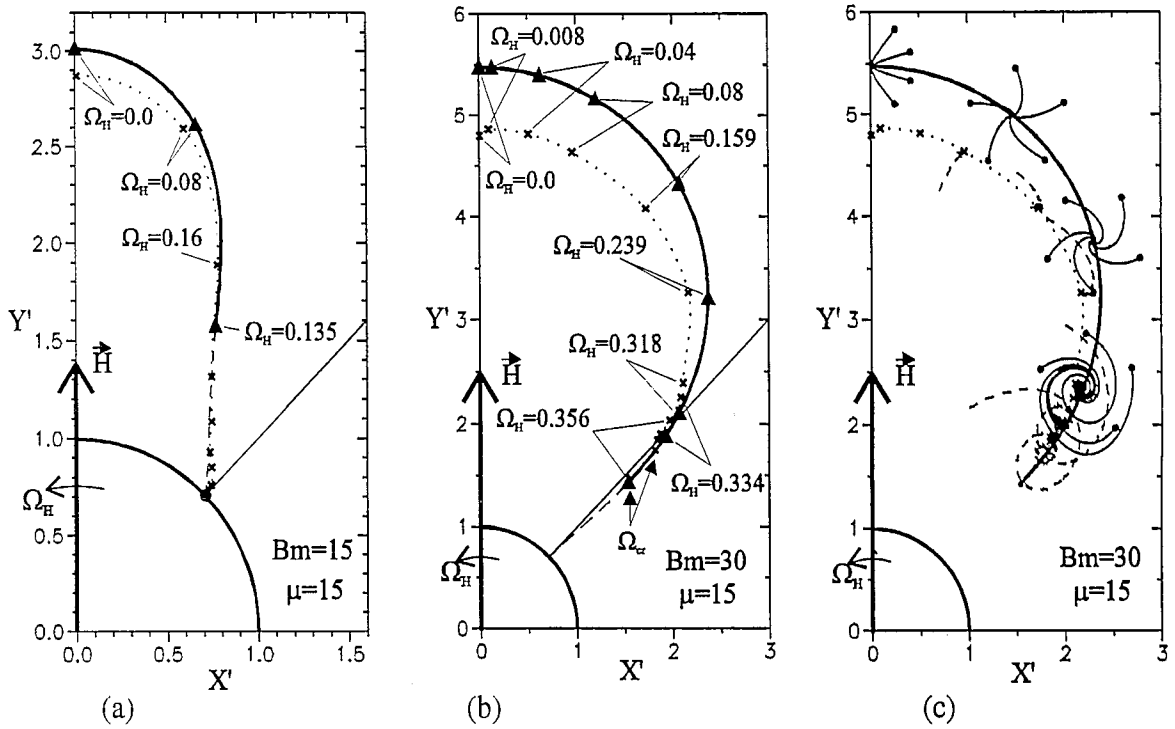

Fig. 2. (a),(b) Steady-state configurations of a MF droplet in a rotating field. (c) Paths leading to the steady state. Results for different field rotation frequencies. Thick solid lines and triangles: simple motion model; dotted lines and crosses: BEM; dashed line in (a), (b): unstable simple model configurations. In (c) thin solid lines are simple model paths to steady state, initial state is given by solid circles; dashed lines are paths calculated by BEM.

$y'_a = a \cos \vartheta$ is taken as the tip. In Fig. 2(a),(b) the solid curve is continued by a dashed one, which corresponds to the unstable simple model configurations. Triangles show the stable configurations at definite frequencies Ω_H. The steady-state configurations obtained by the BEM at definite frequencies Ω_H are shown by crosses, the pointed curve represents the interpolation of these results for a continuously varying frequency Ω_H. In the case of the BEM the most extended point from the centre of the droplet is taken as the tip of the droplet, and the phase lag is calculated for this point. The comparison between the BEM calculations and the simple motion equations calculation shows a fairly good agreement. Discrepancies could be explained by two causes. The first is that the shape of a droplet in BEM calculations (see also Fig. 3) has more rounded tips, and hence the droplet has a smaller extension. The second is that the simple model does not account for the wave-like perturbation propagation on the free

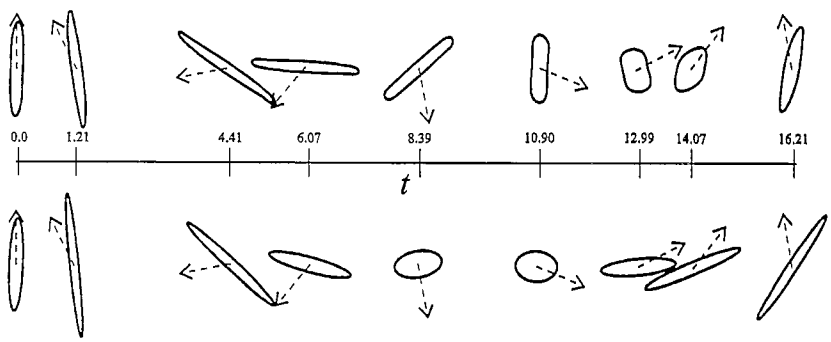

Fig. 3. Series of droplet shapes at fixed time moments for transient motion in laboratory coordinates. The upper series is for the BEM, the lower for the simple model simulation. Dashed arrows represent the field direction; the length of arrow is $3R$.

surface, caused by asymmetric stresses (see Fig. 1(b)). At low values of the elliptic extension ($a < 2$) these stresses cause a motion of the droplet surface which dominates over the pure rotational motion. Thus the simple model simulation shows the lack of stable configurations (Fig. 2(a)) for large field rotation frequencies when a is small.

Two different types of steady-state behaviour are observed (see Fig. 2(a),(b)) depending on the magnetic field strength. These two types are separated by the critical value of the magnetic Bond number, which turns out to be the threshold value of the instability of a 2D droplet in a high-frequency rotating field with respect to the elliptical deformations [9]: $B_{m_{cr}} = 6\pi(\mu+1)^3/(\mu-1)^3$. If the magnetic Bond number is less than the critical one ($B_{m_{cr}} = 28.14$, $\mu = 15$), the extension of the droplet in stationary configurations is diminishing with increase of the rotating field frequency, and the maximal phase lag value $\pi/4$ is reached at infinite frequency as it is shown in Fig. 2(a). For the magnetic Bond numbers larger than the critical one the maximal phase lag ($\approx \pi/4$) is reached already at a finite critical frequency Ω_{cr} (Fig. 2(b)). Phase portraits of the system are presented in Fig. 2(c), they are in accordance with the BEM simulation. As one can see, the dynamics of the droplet in the subcritical range of angular frequencies ($\Omega_H < \Omega_{cr}$) is characterized by the existence of a stable focus, whatever are the initial conditions. In the case of anticlockwise field rotation, the tip of the droplet near the focus rotates clockwise in coordinates (x', y'). The imaginary part of the perturbation decrement when Ω_{cr} is approached is increasing in comparison with the real part, thus causing the rise of the droplet tip rotation around the focus.

In Fig. 3 a transient droplet rotation is shown by a series of droplet shapes and corresponding field orientations. One can see that there is a fair agreement between the simple model and the BEM for large droplet extensions and some discrepancies for small ones. If $B_m > B_{m_{cr}}$ then for large field rotation frequencies ($\Omega_H > \Omega_{cr}$) the motion of the droplet turns out to be jerky and just similarly to the case of the two bound spheres [2,3] it can be characterized as rotation with stops and backward motions. The jerky rotation of the droplet could be described by average angular frequency $\overline{\Omega}$. Fixing the value of a ($\lambda \gg 1$, or $\Omega_H \gg \Omega_{cr}$), the integration of the droplet motion equations gives [3]

$$\overline{\Omega} = \Omega_H - \sqrt{\Omega_H^2 - \Omega_{cr}^2}\,. \tag{15}$$

The value of a could be obtained from the non-linear equation (10) by $\dot{a} = 0$. The results of simple model simulation are shown in Fig. 4 for two different magnetic Bond number values ($B_m = 30$, $B_m = 50$). As one can see, the critical frequency increases with the increase of B_m. Another important conclusion could be drawn about the dependence of the critical frequency on λ: finite values of λ cause stabilization of droplet configurations if the phase

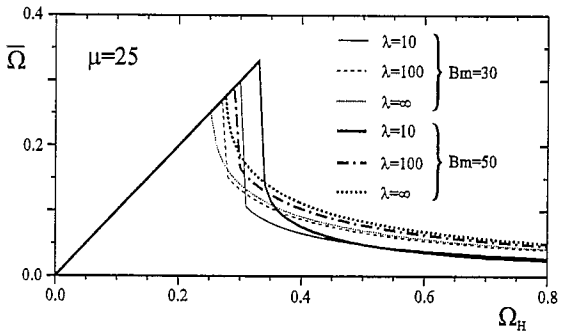

Fig. 4. Plot of the average angular frequency of the droplet rotation versus the field rotation frequency. $\lambda = \infty$ corresponds to the analytical solution for fixed a.

lag ϑ is slightly greater than the critical value $\pi/4$. Increasing λ (the viscosity of the droplet), the critical frequency decreases and tends to its analytical value Ω_{cr} (14). This effect could be explained by the small perturbations from the steady-state configuration a_0, ϑ_0. Denoting the right part functions in Eqs. (10), (14) by $g(a, \vartheta)$, respectively, $h(a, \vartheta)$, the perturbation amplitude depends on time as $\exp((g_a + h_\vartheta)t/2)$, where $g_a = \partial g/\partial a$, $h_\vartheta = \partial h/\partial\vartheta$ at a_0, ϑ_0. Beyond $\pi/4$, $h_\vartheta > 0$, thus the stability criterion is $g_a < -h_\vartheta$. From Eq. (10) it follows that $g_a \propto 1/(\lambda + p)$, hence obviously an increase of λ causes the loss of stability.

Test simulations show that in the case of an elliptic polarized rotating magnetic field, phase locking is found like in Ref. [3].

Acknowledgements: This work was supported by 'Le Réseau Formation Recherche No. 90R0933 du Ministère de l'Enseignement Superieur et de la Recherche' of France. Two of the authors (A.C. and S.L.) are thankful to the International Science Foundation for financial support through long-term grant LBG000.

References

[1] R.E. Rosensweig Ferrohydrodynamics (Cambridge University Press, Cambridge, 1985).
[2] G. Helgessen, P. Pieranski and A.T. Skjeltorp, Phys. Rev. Lett. 64 (1990) 1425.
[3] A.T. Skjeltorp and G. Helgessen, Physica A 176 (1991) 37.
[4] J.C. Bacri, A.O. Cebers and R. Perzynski, Phys. Rev. Lett. 72 (1994) 2705.
[5] A. Cebers, Magnitnaya Gidrodinamika N4 (1986) 3 (in Russian).
[6] J.D. Sherwood, J. Fluid Mech. 188 (1988) 133.
[7] O.A. Ladyzhenskaya, The Mathematical Theory of Viscous Incompressible Flow (Gordon and Breach, New York, 1969).
[8] C. Pozrikidis, Boundary Integral and Singularity Methods for Linearized Viscous Flow (Cambridge University Press, Cambridge, 1992).
[9] J.C. Bacri, A. Cēbers, S. Lācis and R. Perzynski, Magnitaya Gidrodinamika, to appear.
[10] G.F. Jeffrey, Proc. R. Soc. A102 (1922) 161.